Discrete Element Simulation for Polyhedral Granular Particles

Jian CHEN*, Alexander SCHINNER** and Hans-Georg MATUTTIS*

* *Department of Mechanical Engineering and Intelligent Systems, The University of Electro-Communications, Chofu, Tokyo*

** *T-Systems GEI GmbH, München, Germany*

The discrete element method allows the simulation of complex behavior of granular materials without constitutive laws. While in two dimensions shape-effects are well established, in three dimensions there is no universally applicable simulation algorithm for non-spherical particles. We will first present a force model for convex polyhedral particles, using the "overlap" of non-deformed polyhedra as a "measure" of the elastic force and explain the overlap computation algorithm. With this elastic force model, we then show that the continuum-mechanical sound velocity can be recovered for a space-filling packing of cubic blocks. Further, we show simulation results for heaps for which we obtain realistic high angles of repose, which corroborates the reliability of our simulation method and which further more shows that with our method, a larger phenomenology is accessible than with round particles.

1. INTRODUCTION

Granular materials have attracted a great deal of attention of researchers in the last few decades[1, 2, 3], however to date no satisfactory general constitutive relationships have been established. The discrete element method is a suitable tool to study complex behavior of granular materials without constitutive laws[1, 2]. Previous studies showed that in two dimensions the effects of the particle shape on macroscopic properties, e.g. stress-strain relation[4] and sound velocity[5], are significant. Nevertheless, there are hardly any universally applicable simulations for non-spherical soft particles in three dimensions which would give a well-defined force point and force direction, together with the possibility to maintain particle outlines exactly. Radjaï's contact mechanics algorithm allows to simulate rigid polyhedral particles[6], thereby reducing the computational complexity of the contact computations, but due to the "infinite" Young's modulus is not able to investigate any phenomena which are related to finite deformations or propagation speeds. Other groups[7, 8, 9, 10] use the penetration depth as a parameter, but we think that it is difficult to show that for such force laws, the force direction varies continuously when change the orientation of their contact: Each non-continuous direction change will lead to a "blow up" of the simulation, as integrators for the equations of motion need a continuous (or even differentiable) time evolution of the forces. As we have not seen simulations of heaps or free slopes built on smooth grounds with those simulations yet, we are not convinced that such "minimal" force laws can be used in simulations. The model by Smith et al.[11] for quasi-static simulations looks to us like a slight improvement, as it uses the overlap volume as force magnitude. Nevertheless, it uses for the force direction the gradient of the volume overlap, which is difficult to determine in a dynamic simulation, and there is no force point defined which would be necessary to maintain static packings or to introduce static friction.

Another approach is the combination of geometric elements which allow quasi-one-dimensional distance computations , spheres, cylinders and surfaces [12, 13], so that quasi-one-dimensional distance computations can be used, as for spheres. Such "smoothed polyhedra" to our understanding will also suffer from the problem of a not well defined force-points (which are necessary for reliable modeling of static friction) due to the superposition of elements. Moreover, while the surface of such particles may look smooth in the graphics, the superposition of shapes will lead to a rather peculiar variation of the normal force where the shapes overlap: This will lead to a variation of the normal force and the elasticity. When particles slide on top of each other, a particle which slides down a slope modeled in the same fashion may stick even for friction coefficient which should lead to sliding.

A further kind of modelization [14, 15, 16] using three-dimensional Finite-Elements introduces of additional internal degrees of freedom which will make the computational effort more prohibitive than it is already, when one takes into account that a system with 100×100 particles in two dimensions would need $100\times100\times100$ particles in three dimensions. It is also not uncommon that complicated modelization possibilities are described, while the particle geometry in the actual simulations is quite restricted (Latham et al.[15] introduce arbitrary shapes and then simulate cubes).

In this paper, we present a force model for convex polyhedral particles in three dimensions, as well as the algorithm necessary for the computational treatment, and we will show how such a simulation yields the correct sound velocity for space-filling packings. The simulation of heaps constructed by polyhedral particles on a smooth surface shows a well-defined angle of repose as a proof the stability of the simulation method.

2. NUMERICAL SCHEMES

2.1. DISCRETE ELEMENT METHOD

The discrete element method (DEM, see Fig. 1, right) is a method which models interparticle forces based on elasticity parameters and on the overlap of undeformed particle shapes[1, 2]. The penalty-method for the finite element method (FEM) in structural mechanics in contact dynamics simulations uses the overlap of elements in a similar way[17]. Compared to a non-penalty FEM treatment of deformable particles[18], which needs a discretization of the elastic particles, the DEM uses only the degrees of freedom which are necessary for rigid bodies: Three in two dimensions and six in three dimensions. For the accuracy, there are hardly any drawbacks, as the only additional information one could gain from the FEM, internal stresses and strains, are either not of interest, or unreliable due to the fact that the microscopic surface asperities or material inhomogeneities in realistic granular materials like amorphous solids will lead to arbitrary alterations of the FEM-results anyway.

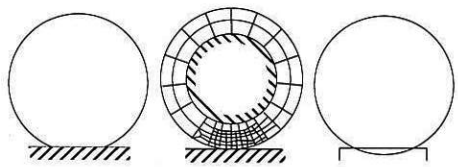

Fig. 1 Physical situation, a soft sphere is deformed while contacting a plane (left) and the simulation with FEM, many degrees of freedom necessary (middle) and the overlapping shapes in DEM, only degrees of freedom of the corresponding rigid body problem necessary (right).

2.2. POLYHEDRAL PARTICLES

Many DEM simulations of granular particles model particles as two dimensional discs. This allows to reduce the problem of identifying a two-dimensional contact situation to a one-dimensional distance calculation. The drawback of this approach is that this simulations are unreliable for dense configurations where the competition between rolling and sliding determines the dynamics of the system. Irregular polyhedral particles can be generated relatively easily by convex-hull-

algorithms[19] of random initial points while more regular shapes can be obtained by choosing the corners on the hull of an ellipsoid with given half radii[20]. The faces of a polyhedral particle are triangles or divided into triangles for computational simplicity.

2.3., EQUATION OF MOTION

The movements of the particles are decomposed according to König's theorem as translational movements of the centers of masses and rotational movements around the centers of masses. For translational movement, Newton's equation of motion

$$M\ddot{x} = F, \tag{1}$$

is applied, where M is the mass matrix, x the position vector and F the force vector. A crucial difference between the linear degrees of freedom and the rotational degrees of freedom is that while translations commute like vector additions, rotations don't commute, like matrix multiplications. For rotational degrees of freedom, we have to use Euler's equation of motion which relates the eigenvalues of the tensor of the moment of inertia I_i, the torques τ_i and the time derivative of the angular velocity vector ω_i as

$$I_1\dot{\omega}_1 - (I_2 - I_3)\omega_2\omega_3 = \tau_1 \tag{2}$$

$$I_2\dot{\omega}_2 - (I_3 - I_1)\omega_3\omega_1 = \tau_2 \tag{3}$$

$$I_3\dot{\omega}_3 - (I_1 - I_2)\omega_1\omega_2 = \tau_3, \tag{4}$$

for the principle axes $i = 1, 2, 3$. While Newton's equation of motion is Galilei-invariant, i.e. it can be solved in any coordinate system, Euler equation of motion must be solved in the center of mass system. In addition, for numerical stability, we use quaternions rather than Euler angles and angular velocities directly to represent orientations and rotational degrees of freedom.

2.4. INTEGRATION: GEAR-PREDICTOR-CORRECTOR

As numerical approximation for the equations of motion, the backward difference formula of fifth order (also called "Gear Predictor Corrector"[21, 22]) is used. The advantage of this method is that it is "stiffly stable", i.e. able to neglect small oscillations in the solution, and "A-stable"[23], i.e. able to approximate the solution of some equations with arbitrary large timestep. Moreover, it is an implicit method which does not need a matrix inversion or a solution of a non-linear system of equations for integrating first or second order differential equations if the predictor-corrector formulation is used. For a comparison, as shown in Fig. 2, the Gear-Predictor-Corrector took much less computational effort than the Runge-Kutta 4/5-th method("Prince-Dormand method", DIFSUB by Gear[21]) to resolve the equilibrium position for the time-adaptive implementation.

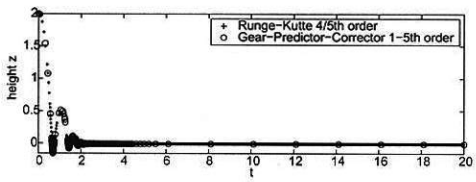

Fig. 2 Simulations of a bouncing ball with gravitation constant $g = 9.8$, mass $m = 1$, damping constant 0.3 and spring constant $k = 10^3$ dropping from height $h = 2$ on a floor: the Gear-Predictor-Corrector method allows much larger timesteps than the Runge-Kutta method.

2.5. GENERAL PROGRAM FLOW

The flow diagram for the simulation of polyhedral granular particles using the predictor-corrector integration algorithm is given in Fig. 3. The simulation starts from an initial state of the system, the position-vector x, the velocity-vector v, the orientations represented by a quaternion array q and the angular-velocity-vector ω. The new positions and orientations are computed

from the Gear predictor formula. These new positions and orientations of the particles are used to update the vertices, edges and faces. From these actual geometric dimensions, the possible contact-particle-pairs are determined. For the interacting pairs, the forces and toques caused by the interaction are computed and inputed into the corrector. This process is iterated until the end of the desired simulation time.

3. CONTACT DETECTION

In principle, for a simulation with n particles, the interactions between one particle with all other $n-1$ particles must be checked. This gives a computational effort of all the particle interactions of the order $n(n-1)/2$. The pre-factor $1/2$ stems from the fact that for a force F_{ij} of particle i on particle j, we have $F_{ij} = -F_{ij}$, thanks to Newton "action-reaction" principle. If the interactions are "long-range", it is necessary to evaluate all these interaction forces directly. Since the interaction in granular material systems are short-ranged, i.e. only contacting particles experience interaction. Instead of checking all possible $n(n-1)/2$ interactions, we need a more efficient algorithm to find the likely contact particle pairs. The overall strategy for contact detection is to start with operations which are "computationally cheap", but inaccurate, and continue with more "computational expensive" operations to reduce the number of contact pairs. To be specific, the "bounding box" method, the "bounding circle/sphere" method and the "projection" method are applied sequentially to first obtain and then refine a contact-particle-pair list for later force and torque computation.

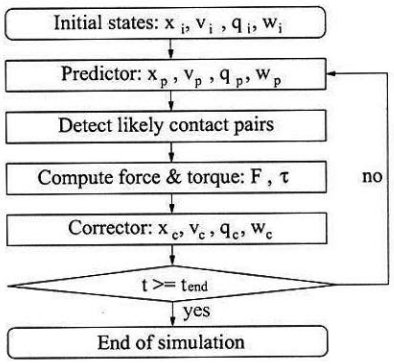

Fig. 3 Flow diagram for the simulation of polyhedral granular particles.

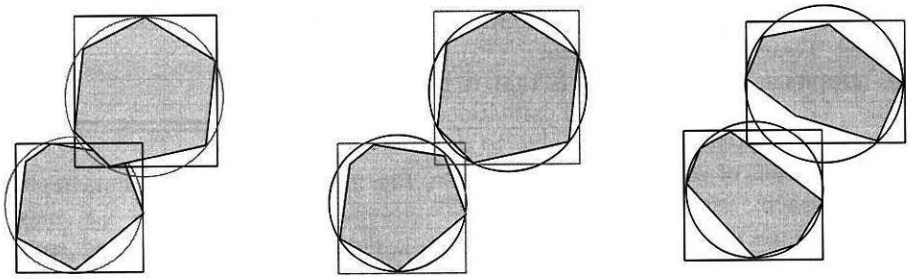

Fig. 4 Left: Intersection of the bounding boxes and the bounding circles, two particles intersect; Middle: Intersection of the bounding boxes while no overlap of the bounding circles, no intersection between the two particles; Right: Intersection of the bounding boxes and circles, no intersection between the two particles.

We first check the extremal coordinates of the particles to find out whether there is an overlap. The extremal coordinates form the "bounding boxes" of the particles (see the rectangles in Fig. 4). If there is an overlap between the bounding boxes of the two particles, we put them in the contact-pair-list. However, the overlap between bounding boxes does not guarantee the overlap between particles, as can be seen in Fig. 4, middle and right. Then we need to check whether there is an overlap between the "bounding circles" of the particles. Bounding circles share the centroids of the particles and have as radii the distances from the centroids to the

furthest vertices (see the circles in Fig. 4). By checking the overlap between the bounding circles, cases like Fig. 4, middle, could be eliminated from the list. For elongated particles like in Fig. 4, right, the overlap test of the bounding boxes and circles could not effectively determine whether two particles would intersect. Therefore we apply a projection method for refining the list. While the overlap of bounding boxes depends on the relative orientation of the particle pair and the coordinate axes, the projection method includes the relative position of the particles directly independent of the axes' orientation. For a pair of particles whose bounding boxes and circles overlap, see Fig. 5, we first connect the centroids of the two particles, $\mathbf{C_1C_2}$, as a baseline. Then we project the vertices of the two particles with respect to their centroids along $\mathbf{C_1C_2}$. This yields the maximal protrusion of $\mathbf{Pr_1}$ from centroid $\mathbf{C_1}$ and $\mathbf{Pr_2}$ from centroid $\mathbf{C_2}$. If $\mathbf{C_1Pr_1}$ and $\mathbf{C_2Pr_2}$ have no overlap, we remove this pair from the contact-particle-pair list. After the refinement by the projection method, for simulating n particles, we obtain a contact-particle-pair list whose number of entry is far less than $n(n-1)/2$.

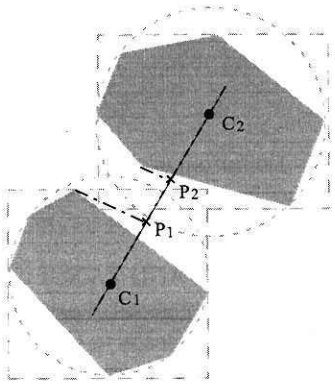

Fig. 5 Projection method: The projected vertices along the connection of the centroids of the two particles do not overlap, the two particles have no intersection.

For simplicity, we have explained the algorithms for contact detection in two dimensions, but the implementation to three dimensions is straightforward. Rectangular bounding boxes become cuboids and bounding circles become bounding spheres. The projection method remains unchanged since it is independent of the choice of axes. If we check the bounding box of each particle with all other particles, the checking itself is still an $O(n^2)$ algorithm. Thus, the incremental sort-and-update algorithm applied by Schinner[24] for polygonal particles was generalized to three dimensions and capable of providing a primitive contact-particle-pair list at low cost for further refinement by checking the bounding spheres and the projections of the vertex-vectors of particle pairs in the list.

4. ELASTIC FORCE MODEL

While the degrees of freedom are integrated out according to the equations of classical mechanics, the physical content of the interaction between particles, see Fig. 6, is a matter of foresightful modeling. When we want to model the interaction between two intersecting particles, we have to define three basic properties: The magnitude of the force, the direction of the force (for forces which are not central forces) and the force point (to define torques). For the simulation of two dimensional polygonal particles, we have a stable elastic force model[4] whose generalization to polyhedral particles in three dimensions is the subject of the following sections.

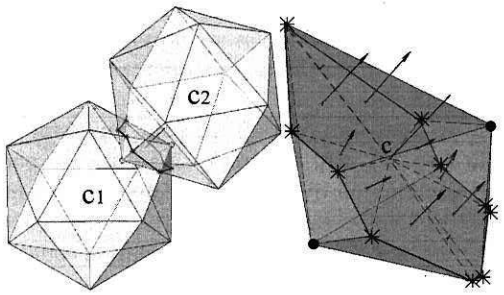

Fig. 6 Two interacting polyhedra (left) and their overlap polyhedron (right): the thick line is the contact line and the vector starting at the center of mass c indicates the direction of the normal force; the vertices with star-maker are generated and with circles are inherited.

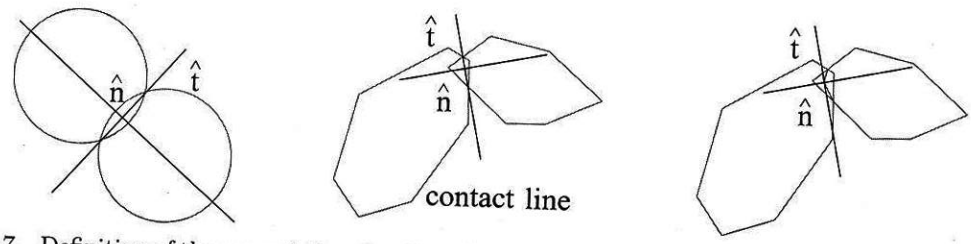

Fig. 7 Definition of the normal direction $\hat{n}$ and tangential direction $\hat{t}$ for two-dimensional particles, circle-particles (left), for polygons via the contact line (middle) and for via the center of mass of the overlap polygon and its connection to the intersection points (right).

4.1. NORMAL- AND TANGENTIAL DIRECTION

For normal collisions of particles, we take into account the deformation and the collision velocity. Tangential sliding leads to Coulomb friction so that we need unique mathematical definitions of the normal- and the tangential force. For round particles, it is common to define the vector connecting the two centers of mass as the normal direction. For polygonal particles, we can use the "contact line", which goes through the two intersection points of the contacting particles, as the tangential direction and its normal as normal direction. Alternatively, one could connect the center of mass of the overlap polygon and the two intersections points to obtain the "contact line", which is actually a connection of two line segments. We take the normals of the two segments and define a unique normal direction by summing up the two normals weighted by their lengths. Accordingly, the direction perpendicular to the normal direction is the tangential direction. For polyhedral particles, the length-weighted normal direction definition becomes area-weighted (Fig. 6, right): First, the contact line is obtained which is a sequential connection of the line segments go through the intersection points; Second, the contact triangles are obtained by connecting the center of mass of the overlap polyhedron and the line segments; Finally, summing up the area-weighted normals of the contact triangles gives the normal direction. The plane orthogonal to the normal direction is the tangential plane in which the friction can be defined.

4.2. ELASTIC FORCE MAGNITUDE AND FORCE POINT

The modeling of forces in normal direction for the DEM borrows from the basic models of elasticity, namely Hook's and Hertz's law (for the elastic force, see Fig. 8). When we model an overlap with the DEM for a bar, the elastic force F_{el} will be proportional to the penetration depth dx. On the other hand, if we want to model the contact of a spherical particle[25], the elastic force F_{el} will be proportional to $dx^{3/2}$. Many simulation codes for round particles exist which make use either of linear or Hertzian potentials. For arbitrary shaped particles, the use of the penetration depth as parameter of the force is not practicable, because taking into account contact shapes (corner-on-corner, corner-on-edge, corner-on-face, edge-on-face, face-on-face) is tedious. For our polyhedral simulation (see Fig. 6) it is more convenient to use as parameter the volume of the overlap region, which can be shown to reproduce the linear regime and the Hertz-regime for the corresponding contact geometries. As force point, the center of mass of the overlap polyhedron can then be used (see Fig. 6). As far as the accuracy of the computation of overlap region is concerned, if we want to calculate the overlap of two cubes along their faces of e.g. 0.01m × 0.01m × 0.01m size, with

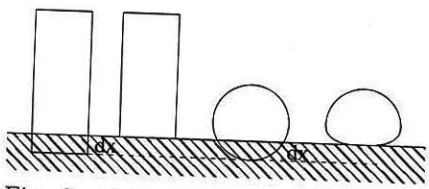

Fig. 8 Deformations and overlap in elastic models: linear contact model (for rectangles, left), and Hertzian contact model (for spheres, right) with penetration depth dx.

realistic Young's modulus of about 100 GPa=10^{11} N/m^2, we get the following estimate: Assuming a weight of 1 g for the particle, the relative penetration depth will be

$$\frac{\Delta l}{l} = \frac{F}{A \cdot Y} = \frac{0.001\text{kg} \cdot 9.81\text{m/s}^2}{0.01\text{m} \cdot 0.01\text{m} \cdot 100 \cdot 10^9\,\text{N/m}^2} \approx 10^{-9}.$$

With double precision (16 digits accuracy), we would have enough digits left so that rounding error will not affect our simulation. For sharper contacts, or softer material, which both result in larger penetration depth, the accuracy problem will become less severe.

The elastic force law (without viscous damping and tangential friction) is a purely position-dependent law, so the energy is always conserved. By orientational changes without volume changes no additional energy can be "created" or "destroyed" in the system. We used the energy-conservation as one of the first confirmations for the correctness of our simulation when we debugged the code: Particles which dropped on a surface seemed to rotate rather fast after the collision with the ground or other particles, but by monitoring the (conserved) energy, we saw that the rotation was actually physical. The impression that the rotation is unphysical came from a lack of actual "experience": Real particles which start rotating after a collision move too fast for the free eye. The seeming "singular" shapes (corners, edges) behave "singular" during interaction only inasmuch contacting particles at sharp contacts prefer to twist towards either one side or the other: The time evolution of the force (magnitude and direction) is nevertheless smooth.

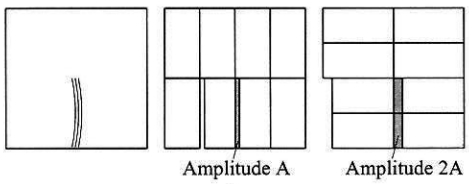

Fig. 9 Sound wave in the continuum (wavy line, left), in a packing of cubes (shaded overlap region of particles, middle) and of parallelepipeds (right).

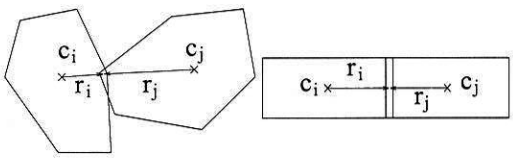

Fig. 10 Vectors from the center of mass c_i, c_j to the contact point for arbitrarily shaped (left) and regular (right) particles.

4.3. CHARACTERISTIC LENGTH

While our interaction should locally reproduce the contact laws depending on the shape of the contacting particles, we should take into account the units. If we use Young's modulus (unit: N/m^2) multiplied with the volume of the overlap polyhedron (unit: m^3), there is still a factor L with a unit of length missing. The sound velocity in bulk solids is a physical property can be used to fix this length factor analogously to the two dimensional polygonal model[5]. Sound waves (microscopic deformations of the continuum traveling at sound speed c which is only material-dependent, not e.g. amplitude-dependent) are mimicked in DEM-simulations by microscopic displacements of the center of mass of the particles which should propagate with c for space-filling packings. Space-filling packings of cubes or parallelepipeds should have the same sound velocity as the bulk continuum, $c_{bulk} = \sqrt{Y/\rho}$, which should depend only on the material parameters, namely the density ρ and Young's modulus Y. Obviously, if we would choose the factor L constant, we see in Fig. 9 that a sound wave/overlap amplitude in a packing of "short" particles would lead to smaller accelerations than a larger amplitude for "longer" particles. Thus instead of using a constant length factor, which makes the sound velocity dependent on the particle size, we define the "characteristic length" L_c for two intersecting particles i and j with arbitrary shapes of different "radii", $|r_i|$ and $|r_j|$ (distance between center of mass and contact point Fig. 10, left):

$$L_c = 4\frac{|r_i||r_j|}{|r_i| + |r_j|}.$$

This definition, for two rectangular particles of the same shape contacting with parallel sides, gives exactly the length of the particle (Fig. 10, right). With the definition of the "characteristic length", we finally have the complete form of elastic force magnitude: $F_e = YV_{overlap}/L_c$.

The characteristic length is therefore a quantity which has to be introduced to make the sound velocity in granular materials independent of the particle size. It serves to compensate the "time of flight" which the sound wave would spend while it passes through the particle, distant from the inter-particle contacts. This is not an effect of our choice of force law: Also for packings of spheres, one has to assume that the sound velocity should not change with the particle size, but with the packing density. The characteristic length is therefore complementary to the force-law (linear, Hertz or whatever): While the force-law takes care of the microscopic interaction at the contact point, the characteristic length takes care of the macroscopic propagation speed of this interaction through the bulk.

4.4. OVERLAP COMPUTATION

To compute the elastic force between two contacting polyhedra, we need to obtain the geometry of the overlap region, including its vertices, edges and faces. There are two types of vertices, inherited and generated. Inherited vertices are vertices of one polyhedron which penetrate into the other polyhedron, while the generated vertices are the intersection points of the triangulated faces of the two polyhedra, see Fig. 6, right. Here we will shortly outline the way to determine the inherited vertices. A plane with unit normal $\mathbf{n}(n_x, n_y, n_z)$ is represented in point normal form as

$$\mathbf{n} \cdot \mathbf{r} - d = 0, \tag{5}$$

where $\mathbf{r}(r_x, r_y, r_z)$ is an arbitrary point on the plane and d the distance from the origin to the plane. If the normals of the all the faces of a polyhedron point outside, any points $\mathbf{r}'(r'_x, r'_y, r'_z)$ located inside the polyhedron should satisfy the inequality

$$\mathbf{n}_k \cdot \mathbf{r}' - d_k < 0, \tag{6}$$

where the subscript k indicates the k-th face of the polyhedron. The vertices of the original polyhedra which satisfy Eq.6 are inherited vertices.

For the generated vertices, as indicated by the star markers in Fig. 6, we have to compute the intersection of the triangular faces of the two polyhedra. If the two triangles intersect, the intersection will be a line segment whose endpoints we will call "intersection points". For the degenerate cases, where i) there is only one intersection point or ii) the two triangles are on the same plane or iii) one edge of one triangle is on the plane of the other triangle, in the context of intersection of granular particles, the two particles are either about to start intersecting or separate after they have intersected, so the volume of the overlap region is zero. From here on, we discuss the non-degenerate case. The equation of a line which passes through point $\mathbf{A}(A_x, A_y, A_z)$ and $\mathbf{B}(B_x, B_y, B_z)$ (equivalent to a vector $\mathbf{AB} = \mathbf{B} - \mathbf{A}$) can be written as $\mathbf{r} = \mathbf{A} + \lambda(\mathbf{AB})$, where $\mathbf{r}(r_x, r_y, r_z)$ is an arbitrary point on the line. Substituting this equation into Eq. 5, gives the solution for the parameter

$$\lambda = \frac{d - \mathbf{n} \cdot \mathbf{A}}{\mathbf{n} \cdot (\mathbf{AB})}, \tag{7}$$

for $\mathbf{n} \cdot \mathbf{AB} \neq 0$. In case that $\mathbf{n} \cdot \mathbf{AB} = 0$, $\mathbf{AB}$ is on the plane. For $0 < \lambda < 1$, $\mathbf{r} = \mathbf{A} + \lambda(\mathbf{AB})$ denotes the intersection between the segment $\mathbf{AB}$ and the plane.

For two triangles T_1 and T_2 lying on the planes P_1 and P_2 (Fig.11), we compute the intersection as follows:

Step 1: Compute the three λ (according to Eq.7) for T_1 and P_2, if less than two λ satisfy $0 < \lambda < 1$, exit with no intersection; else two intersection points $\mathbf{V}_{i1}$ and $\mathbf{V}_{i2}$ are obtained;

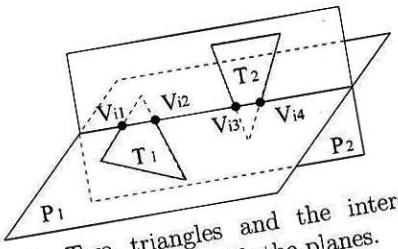

Fig. 11 Two triangles and the intersection points of the triangles with the planes.

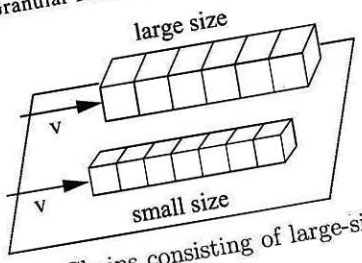

Fig. 12 Chains consisting of large-size and small-size particles

Step 2: Compute the three λ for T_2 and P_1, if less than two λ satisfy $0 < \lambda < 1$, exit with no intersection; else two intersection points $\mathbf{V}_{i3}$ and $\mathbf{V}_{i4}$ are obtained;

Step 3: Sort points $\mathbf{V}_{i1}$, $\mathbf{V}_{i2}$, $\mathbf{V}_{i3}$ and $\mathbf{V}_{i4}$ lying on the same line: if $\mathbf{max}(\mathbf{V}_{i1}, \mathbf{V}_{i2}) < \mathbf{min}(\mathbf{V}_{i3}, \mathbf{V}_{i4})$ or vice versa, no intersection; else, the two middle points in the sorted list are the intersection points.

When all vertices of the overlap polyhedron have been computed, it is easy to rearrange them into edges and faces and then obtain its volume, center of mass and the normals of the contact triangles, as show in Fig. 6. The elastic force is then fully determined.

5. SIMULATION RESULTS

5.1. SOUND PROPAGATION

As discussed in Section 4.3, for a linear chain of particles, a valid elastic force model should be able to reproduce the sound velocity of a bulk with the same kind of material. Deviations will occur if the sound propagation excites resonances of particles due to the effective inter-particle contact strength and the particle mass. We set up two chains consisting of 400 particles, one chain with particles two times larger than the other chain along the sound propagation direction, see Fig. 12. The Young's modulus is chosen as $Y = 2 \times 10^7\,\mathrm{N/m^2}$ and density as $\rho = 5000\,\mathrm{kg/m^3}$, which gives a continuum sound velocity of $c_{bulk} = 63.25\,\mathrm{m/s}$. The chains are triggered by the impact velocity of the first particle during the initial time step. The propagation of dislocations in the chain is sketched in Fig. 13. As can be seen from Fig. 14, the sound velocities of both chains converge to c_{bulk}. The increase of the sound velocity should not be confused with a violation of momentum conservation: The initial impacts and collisions lead to larger movement of the centers of mass of the particles than the finally obtained sound velocity in the chain, where nearly only the dislocation propagates.

5.2. ANGLE OF REPOSE

To apply our algorithm to the investigation of macroscopic properties of granular systems with particles of relatively complicated geometries, we simulate construction of heaps by pouring particles on a smooth, flat floor (modeled as one particle) and measure their angles of repose. The granular particles are generated by choosing corners randomly on the hull of an ellipsoid with half radii 8 mm, 7 mm and 6 mm. Each particle consists of 12 corners and 20 faces and each heap is made up of 1900 particles. The Young's modulus is chosen as $Y = 6.5 \times 10^7\,\mathrm{N/m^2}$ and density as $\rho = 1000\,\mathrm{kg/m^3}$. The Cundall-Strack friction model[1)] is adapted to three dimensions. The coefficient of friction is chosen as 0.6, for both particle-particle interaction and particle-floor interaction. For integrating the equations of motion, Gear's fifth order predictor-corrector is used with a fixed timestep of $dt = 1 \times 10^{-5}\mathrm{s}$. During the simulation, the particles are added batch by batch, as shown in Fig. 15 with scale in centimeter, close to the apex of the heap to reduce the total input energy to the system (otherwise it would take longer time for the system to damp out

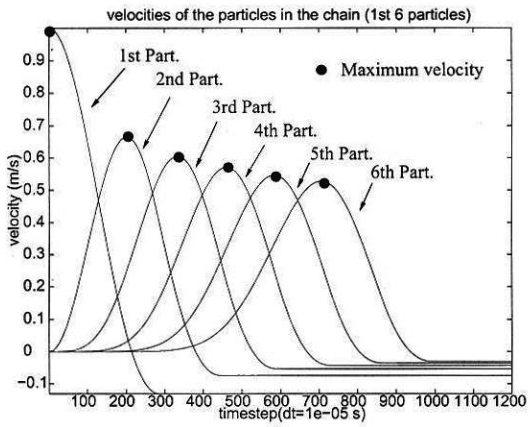

Fig. 13 Propagation of the maximum velocities of the 1st 6 particles in the chain

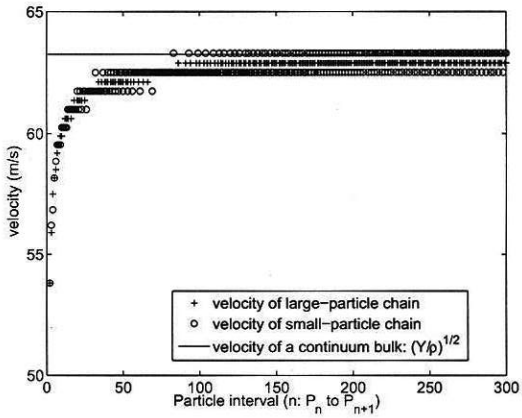

Fig. 14 Sound velocities of the small-particle and the large-particle chain

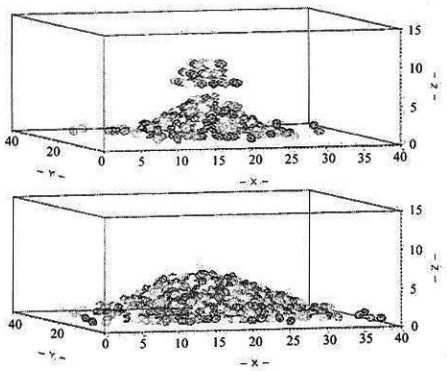

Fig. 15 A heap of polyhedral particles: New batch added (above) and the final stage (below)

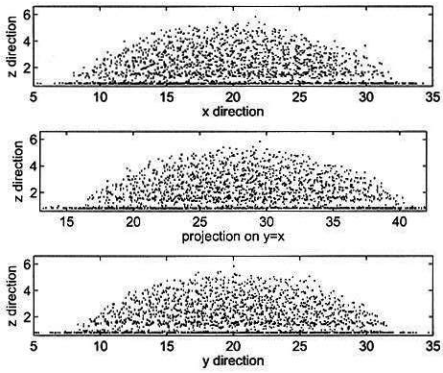

Fig. 16 Angle of repose of one heap views from the y=0, y=x and x=0 plane

the energy of the impacting particles before reaching the equilibrium). A screenshot of the end of one simulation can be seen in Fig. 15 with scale in centimeter. The positions of the centroids of the particles projected into the y=0, y=x and x=0 plane are drawn in Fig. 16. The averaged angle of repose from the simulations is about 30° for five runs of particle geometries generated with different random seeds. Because the number of corners/faces is relatively large, and the particles are inscribed in "nearly" rotational ellipsoids, the angle of repose is smaller than for many technical materials, Nevertheless, it is larger than the angle of repose for round particles (about 22°[26]).

6. SUMMARY AND CONCLUSION

In this paper, we have outlined a implementation of a novel simulation method for polyhedral particles. For the contact detection, we have combined the usage of bounding boxes and bounding circles (spheres) and the projection of vertices along the connection of centroids of particles to provide a small number of contact pair candidates; For the computation of force and torque, we have implemented an elastic force model of polyhedral contacts in three dimensions with an algorithm for the overlap computation. We also performed simulation runs and computed physical

observables. The simulations of granular chains reproduced the sound velocity of the continuum with the same density and Young's modulus, which validates the model from the point of view of continuum mechanics. The simulations of heaps gave realistic high angles of repose which are not usually seen in simulations of spherical particles. This algorithm will be used to investigate practical problems like the dynamics of railway ballast where the influence of the particle geometry cannot be ignored.

ACKNOWLEDGEMENT

The authors acknowledge the cooperation and financial support of the Japanese Railway Technical Research Institute, Tokyo.

REFERENCES

1) Cundall, P. A. and Strack, O. D. L., "A discrete numerical model for granular assemblies", *Geotéchnique*, 29(1), (1979), pp. 47–65.
2) Matuttis, H. G., "Simulation of the Pressure Distribution under a Two Dimensional Heap of Polygonal Particles", *Granular Matter*, 1, (1998), pp. 83–91.
3) Chen, J., Watanabe, L., Matuttis, H.-G., and Sakaguchi, H., "History Dependence of the Density Distribution on Granular Heaps", in M. Nakagawa and S. Luding, editors, "Powders and Grains 2009, Proceedings of the 6th International Conference on Micromechanics of Granular Media", pp. 199–202 (AIP, Golden, Colorado, 2009).
4) Shourbagy, S. A. E., Morita, S., and Matuttis, H. G., "Simulation of the Dependence of the Bulk-Stress-Strain Relations of Granular Materials on the Particle Shape", *J. Phys. Soc. Jpn.*, 75(10), (2006), pp. 104602(1–10).
5) Shourbagy, S. A. E., Okeda, S., and Matuttis, H. G., "Acoustic of Sound Propagation in Granular Materials in One, Two, and Three Dimensions", *J. Phys. Soc. Jpn.*, 77(3), (2008), pp. 034606(1–5).
6) Saussine, G., Azéma, E., Perales, R., and Radjaï, F., "Compaction of Railway Ballast During Tamping Process: A Parametric Study", in M. Nakagawa and S. Luding, editors, "Powders and Grains 2009, Proceedings of the 6th International Conference on Micromechanics of Granular Media", pp. 469–472 (AIP, Golden, Colorado, 2009).
7) Muth, B., Eberhard, P., and Luding, S., "Simulation of Contacting Spatial Polyhedral Particles", in T. A. Kowalewski and W. Gutkowski, editors, "Proceedings of the 21st International Congress of Theoretical and Applied Mechanics", (Springer, Warsaw, Poland, 2004).
8) Muth, B. and Eberhard, P., "Investigation of Large Systems Consisting of Many Spatial Polyhedral Bodies", in D. van Campen, M. Lazurko, and W. van der Oever, editors, "Proceedings of the ENOC-2005 Fifth EUROMECH Nonlinear Dynamics Conference", pp. 1644–1650 (Eindhoven, The Netherlands, 2005).
9) Zhao, D., Nezami, E. G., Hashash, Y. M., and Ghaboussi, J., "Three-dimensional discrete element simulation for granular materials", *Engineering Computations*, 23(7), (2006), pp. 749–770.
10) Nezami, E. G., Hashash, Y. M., Zhao, D., and Ghaboussi, J., "Simulation of front end loader bucketoil interaction using discrete element method", *Engineering Computations*, 31(9), (2007), pp. 1147–1162.
11) Smith, K. C., Fisher, T. S., and Alam, M., "Quasi-static Compaction of Polyhedra by the Discrete Element Method", in M. Nakagawa and S. Luding, editors, "Powders and Grains 2009, Proceedings of the 6th International Conference on Micromechanics of Granular Media",

pp. 90–93 (AIP, Golden, Colorado, 2009).
12) Alonso-Marroquín, F., Galindo-Torres, S.-A., Tordesillas, A., and Wang, Y., "New Perspectives for Discrete Element Modelling: Merging Computational Geometry and Molecular Dynamics", in M. Nakagawa and S. Luding, editors, "Powders and Grains 2009, Proceedings of the 6th International Conference on Micromechanics of Granular Media", pp. 825–828 (AIP, Golden, Colorado, 2009).
13) Wang, J., Yu, H. S., Langston, P., and Fraige, F., "Particle Shape Effects in Discrete Element Modelling of Cohesive Angular Particles", *Granular Matter*, online first.
14) Munjiza, A., The Combined Finite-Discrete Element Method (John Wiley, 2004).
15) Latham, J.-P. and Munjiza, A., "The Modelling of Particle Systems with Real Shapes", *Phil. Trans. R. Soc. Lond. A*, 362, (2004), pp. 1953–1972.
16) Wicke, M., Botsch, M., and Gross, M., "A Finite Element Method on Convex Polyhedra", *Computer Graphics Forum*, 26(3), (2007), pp. 355–364.
17) Wriggers, P., Computational Contact Mechanics, 2nd ed. (Springer, 2006).
18) Zienkiewicz, O. C. and Taylor, R. L., The Finite Element Method for Solid and Structural Mechanics, sixth ed. (Elsevier, 2005).
19) Barber, C. B., Dobkin, D. P., and Huhdanpaa, H. T., "The Quickhull algorithm for convex hulls", *ACM Trans. on Mathematical Software*, 22(4), (1996), pp. 469–483, http://www.qhull.org.
20) Schinner, A. (1995), "Numerische Simulationen für granulare Medien", Master's thesis, Universität Regensburg.
21) Gear, C. W., Numerical Initial Value Problems in Ordinary Differential Equations, Prentice-Hall Series in Automatic Computation (Prentice-Hall, 1971).
22) Allen, M. P. and Tildesley, D. J., Computer Simulation of Liquids (Clarendon Press, Oxford, 1987).
23) Hairer, E. and Wanner, G., Solving Ordinary Differential Equations II Stiff and Differential-Algebraic Problems, second revised ed. (Springer, 1996).
24) Schinner, A., "Fast algorithms for the simulation of polygonal particles", *Granular Matter*, 2, (1999), pp. 35–43.
25) Johnson, K. L., Contact Mechanics (Cambridge University Press, 1985).
26) Albert, R., Albert, I., Hornbaker, D., Schiffer, P., and Barabási, A.-L., "Maximum angle of stability in wet and dry spherical granular media", *Phys. Rev. E*, 56(6), (1997), pp. R6271–R6274.